(Commercial)

Harpur Hill, Buxton
Derbyshire, SK17 9JN
T: +44 (0)1298 218000
F: +44 (0)1298 218986
W: www.hsl.gov.uk

HEALTH & SAFETY LABORATORY

ETI High Hydrogen Contract
Work package 2.2 – Part 2 of HSL report
Detailed Analysis of Results

MHU-15-138

Hans J. Michels, Drs,PhD,DIC,CEng,CPhys,FInstP,
Professor of Safety Engineering

Stuart J Hawksworth, PhD

DISTRIBUTION

Paul Winstanley ETI
Andrzej.Pekalski Shell
Hans Michels Imperial London
Bruce Ewan

John Gummer HSL
Keith Moodie HSL
Wayne Rattigan HSL
Louise O'Sullivan HSL
Stuart Hawksworth HSL
Rosemary Gibson HSL

CONTENTS

EXECUTIVE SUMMARY

This Report (WP2, Task 2 Part 2) is concerned with the analysis and discussion of the first set of results from Work Package 2, Task 2 of the ETI contract PE0202 “High-Hydrogen (HyH) Project” obtained at the HSL, Harpur Hill Buxton, between autumn 2014 and summer 2015. Full details of the facilities used and tests carried out can be found in “ETI WP2, Task 2 Report Part 1. Experimental results.[MH_15_138]

In Section 1 of this report the results database of the full set of 61 tests on the three component $H_2/CH_4/CO$ fuel system are used to establish the lowest hazardous and highest safe fuel-air mixture concentrations for turbine exhaust streams passing through model heat exchanger type obstructions.

Section 2 considers the primary evidence from the 61 tests on the impact the presence of heat exchangers models has on the character of the combustion process and identifies a selection of mixtures most suitable for more detailed analysis. Limitations to this investigation as result of the technical challenges associated with large scale facility and known limitations of the instrumentation are listed. Details and required scope of a review of the data presented to date are discussed.

Section 3 outlines the procedure to extract relevant information from the available results. Appendix A gives greater detail on these procedures, providing a step by step process and is illustrated with a detailed account of the analysis of one of the primary test results from the experimental WP2.2 programme

Section 4 presents the results of such analysis of 5 core tests for the delivery of the intermediate objectives of the programme which has culminated in distance vs time diagrams as a base for further forthcoming work in both WP2.2 and WP2.3.

Section 5 evaluates the meaning of the findings, emphasising both more fundamental confirmation of the general lessons from the work of Section 1 and important advice for the WP2.3 programme.

Section 6 identifies potential further analysis that is recommended to ensure the maximum information is obtained from WP2.2.

1 THE SAFE OPERATING MODES FOR $H_2/CH_4/CO$ MODEL FUEL MIXTURES.

As indicated in previous documentations and discussed at stage gate meetings, information on the upper concentration safety limit for the use of model high hydrogen content gas mixtures in the circular duct facility of work package WP2.2 was to be obtained by investigating the influence of an increase in the equivalence ratio (EQR) of selected fuel mixes on flame velocities and generated overpressures.

In summary, eight fuel mixture compositions were selected for these tests:

(1) 100% H_2 - 100% CH_4 - 100% CO;
(2) H_2/CH_4 60/40 - H_2/CH_4 40/60;
(3) H_2/CH_4 60/40 – H_2/CH_4 40/60;
(4) H_2/CH_4/CO 40/25/35

For each of these mixtures

(a) Normally three EQRs would be tested to record flame behaviour across anticipated safe-unsafe boundaries. Starting EQR choices for such tests were based on results from the WP2, Task 1 Imperial College laboratory tests; subsequent choices were made in the light of last experience.
(b) This procedure was carried out with, and without flow obstruction, with the obstruction provided by a model heat exchanger (MHE) arrangement of respectively 8 and 15 rows of tubes.
(c) To simulate as closely as possible real-life conditions, the tests were carried out with the lowest flow entry velocities (≈ 20 m/s) that could be achieved with the circular duct facility (≈ 20 m/s). Unfortunately but not critically this failed to be as low as in real life situations (4 – 8 m/s).
(d) A few tests were carried out at lower temperature, to appreciate the sensitivity of results on this parameter.
(e) Higher exhaust flow velocity tests, essential for predicting WP2, Task 3 conditions were deferred.

The full list of all tests for (a) – (d) above can be found in the HSL's Experimental Report. Because of the exploratory nature of the work, the tests were not carried out in a fully arranged order of the investigated fuel mixtures. For the purpose of this report results have been rearranged as shown in Table 1.
Safety conclusions from these tests are mainly focussed on the over-pressures generated. As could be expected, the highest over-pressures were found in tests with the longest (15 rows of tubes) heat exchanger model. For all eight

systems investigated with the complete MHE system, the corresponding over-pressures as a function of EQR are listed in column 6 of Table 1.

Table 1: Stream Fuel mixtures, EQRs, overpressures, flame velocities and temperatures from the WP2.2 circular duct test programme. (Uncorrected data from the HSL Experimental Report)

Mixture	**Run**	**EQR**	**----------ΔP---------- (mbar)**				**V_{max} [m/sec]**	**T_{max} [K]**
			0 rows	**8 rows**	**15 rows**	**15 rows (low temp)**		
H2-100%	22	0.32		0			0	855
	63	0.35				374	185	567*
	23	0.40		0			0	892
	41	,,			0		0	1017
	9	0.42	73				93	760
	28	,,			451		167	779
	42	,,			1400		278	850
	62	,,				788	250	616*
	61	0.50				2230	769	898
	10	0.51	130				115	839
	44	,,			1762		286	847
	24	0.52		323			219	815
	27	0.53			1733		417	827
	43	0.60			9400		1724	93
	26	0.63		1950			288	874
	29	,,			7159		1875	939
	25	0.71		7620			2500(?)	958
	11	0.72	320				348	992
H_2/CH_4 60/40	13	0.35	43				63	779
	19	0.36		75			49	711
	66	0.40				84	89	619*
	65	0.50				1579	312	720*
	30	0.55			284		208	1139
	64	0.58				2774	694	792*
	31	0.65			3016		556	971
	5	0.67	168				196	992
	20	,,		591			353	969
	21	0.81		1670			451	1109
	12	0.87	262				357	779
	7	0.88	204				312	1172
	8	,,	205				310	1092

Table 1 (continued):

Mixture	Run	EQR	----------ΔP---------- (mbar)				V_{max} [m/sec]	T_{max} [K]
			0 rows	8 rows	15 rows	15 rows (low temp)		
H_2/CH_4-40-60	38	0.60			363		357	997
	39	0.61			600		242	944
	36	0.65			416		313	988
	40	0.66			1353		233	996
	37	0.75			1515		391	1057
CH_4-100%	35	0.65			300		227	1058
	34	0.76			650		548	1078
	33	0.86			2620		595	1111
	4	1.00	232				312	1172
	1	1.02	230				392	869
	2	,,	216				240	1182
	3	,,	209				366	1172
H_2/CO-60/40	53	0.40			218		129	800
	54	0.50			1500		286	842
	56	0.56			966		185	824
H_2/CO-40/60	50	0.41			227		176	845
	17	0.50	Pre-ig					
	18	,,	Pre-ig					
	16	,,	91				90	858
	52	,,			824		286	1046
	67	,,				1075	366	881*
	15	0.55	Pre-ig					
	49	0.65			10380		2500	1218
CO-100%	14	0.35	Pre-ig					
	46	0.44			130		158	705
	47	0.60			574		417	1181
	48	0.77			3000		1000	1268
H_2/CH_4/CO 40/25/35	60	0.45			214		96	720
	59	0.51			1500		275	899
	58	0.56			1503		313	1029
	57	0.65			3128		385	1308

Note: Test 14,15,17 and 18 pre ignited.

The same information is also given in Figures 1.(a – c). As reactivity tends to increase exponentially with concentration, the vertical axes of the diagrams have a logarithmic scale, which allows trends to be approximated with straight lines.

The maximum over-pressures recorded were almost always not at EQR levels that represent the lower and upper limits respectively of hazardous and safe operating conditions, i.e.: those causing respectively unacceptably high or acceptable over-pressures from unintended ignition of not-combusted CCTG or

CCGE exhaust flow. What these limits are in practice will depend on a number of factors.

(i) The results of Figures 1 do not lie all on a single line; even a power trendline could not achieve that. For the high overpressures this is in a minor part due to the accuracy of the recordings. Overwhelmingly it reflects the stochastic nature of the combustion process especially in such turbulent environments. For the definition of practical safety margins, the hazardous limit can only be set against the lowest EQR for which unacceptable over-pressures are recorded.

(ii) The extent of a practical Δ-EQR safety margin will first of all depend on the stability of the composition of the industrial process stream which in turn is decided by the nature of the process. Waste gas streams are likely to be less reliable than process discharges. Increasing the concentration of generated hydrogen will increase stability.

(iii) Another important consideration is what the maximum pressure excursion is that the industrial facility can accommodate without being damaged and whether a distinction needs to be made between very short duration pressure peaks and more extended pressure waves. Quite apart from metal choice and wall thickness, ductile materials tend to stand up better to the former than brittle ones, the shock sensitivity and accuracy of recording instruments can be very dependent to both.

(iv) Finally environment and operator preference may be deciding factors. In congested areas there is limited scope for relief and venting. Location, guaranteed operator availability and skills, industrial and national safety standards may all be of influence.

However, from advisory comments received during the project it was provisionally concluded that over-pressures above 3 bar would be likely to cause permanent damage to some part of the installations, while 0.4 bar was generally regarded as safe and otherwise acceptable. These over-pressure levels have been indicated on the diagrams of Figure 1.

Figure 1.(a): H_2/CH_4

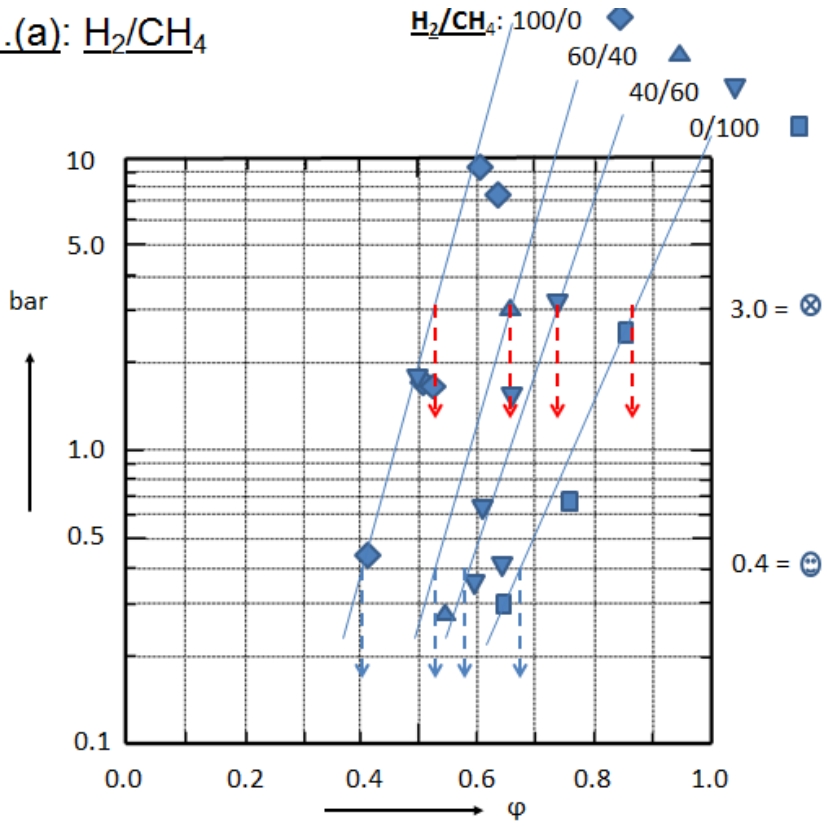

Figure 1(b): H_2/CO

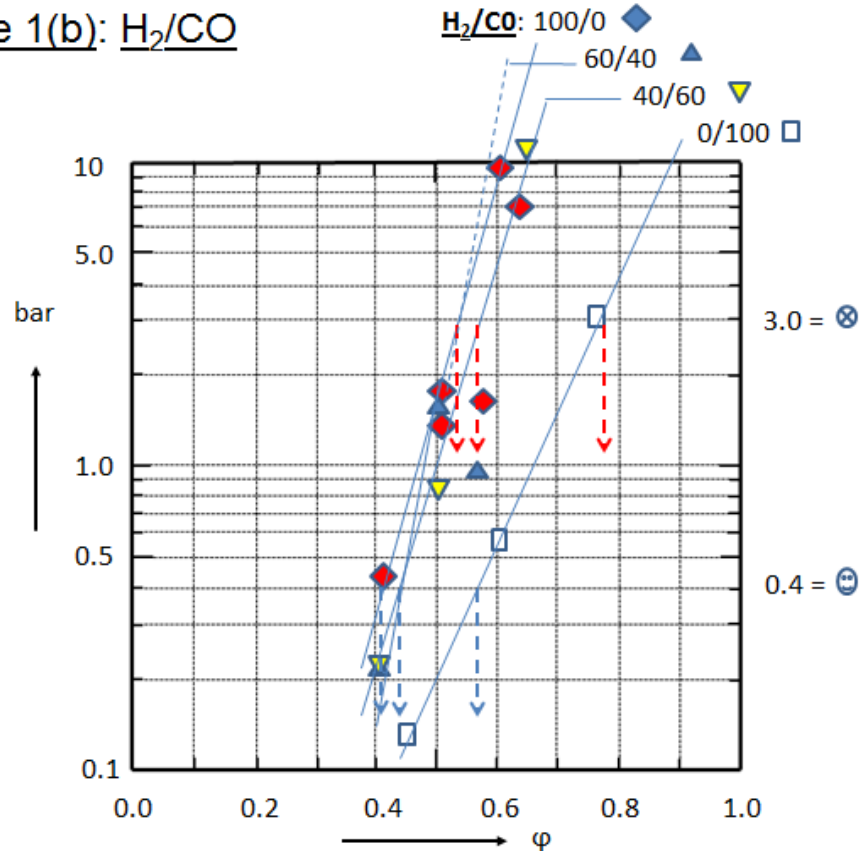

Figure 1(c): $H_2/CO/CH_4$

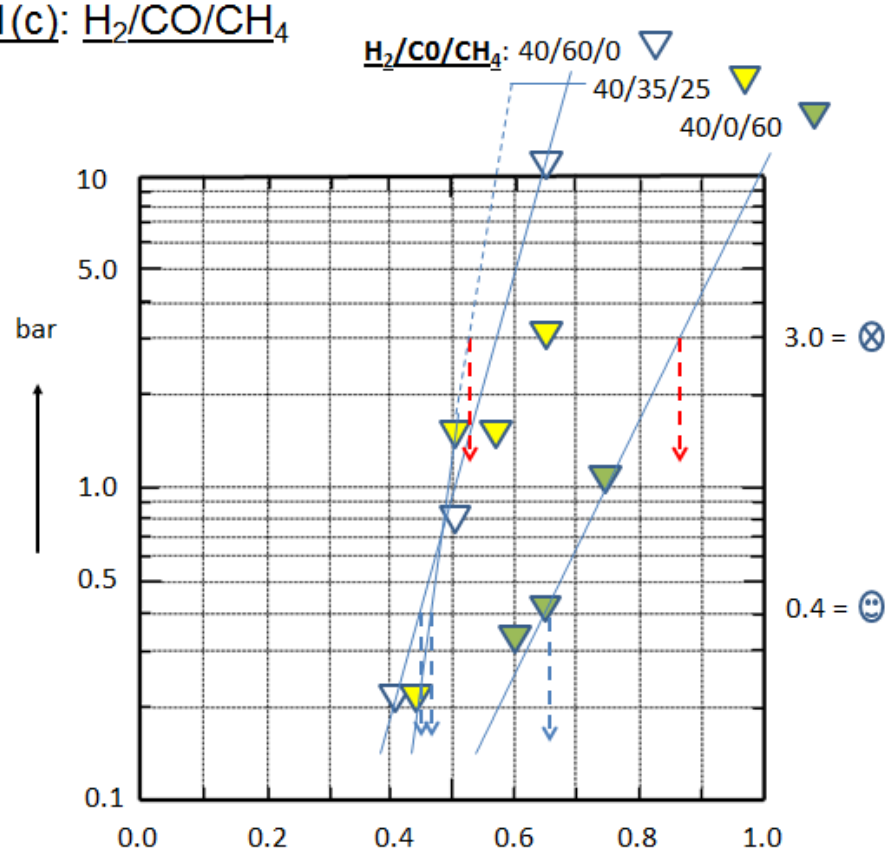

The conclusions from Figures 1 are summarised in Table 2. It shows that the EQR gap between the two identified levels varies from about 0.10 to 0.20. Given the uncertainties listed above and the general ability to control fuel mixture composition and all times, it would seem reasonable to assume a safe gap at the higher 0.20 Δ-EQR level. This results in the recommendation of Table 2, column 5.

The data from Table 2 have also been used to construct the trapezoid diagram of hazardous and safe operating planes previously anticipated at Stage Gate 3 and in VAR027 and here shown as Figure 2.

Table 2: Equivalence ratios of model fuel mixtures for respectively "highest safe" and "lowest hazardous" concentrations in air and recommendations for safe operating EQR of these mixtures in practical situations.

Fuel Mixture	EQR $_{0.4\ bar}$	EQR $_{3.0\ bar}$	Δ EQR	Recommended max. EQR for safe operation.
100% H_2	0.41	0.53	0.12	0.35
H_2/CH_4 60/40	0.53	0.67	0.14	0.45
H_2/CH_4 40/60	0.58	0.74	0.16	0.55
100% CH_4	0.67	0.86	0.19	0.65
H_2/CO 60/40	0.43	0.53	0.10	0.35
H_2/CO 40/60	0.44	0.57	0.13	0.35
100% CO	0.57	0.77	0.202	0.55
$H_2/CO/CH_4$ 40/35/25	0.45	0.55	0.10	0.35

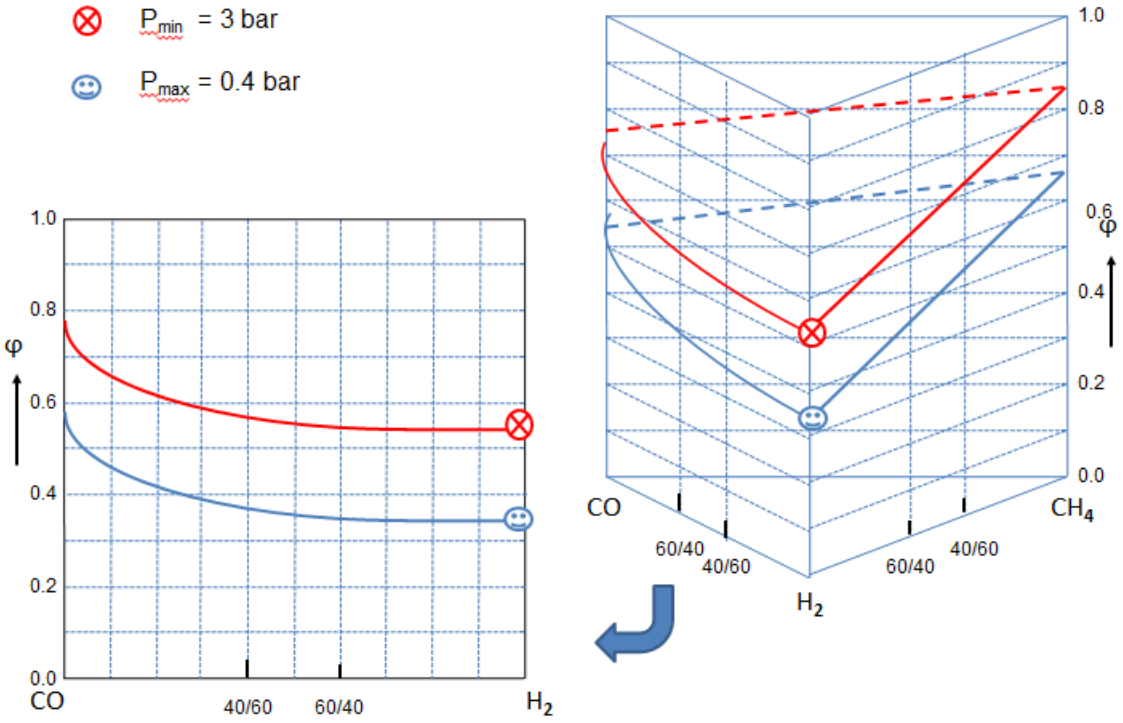

Figure 2: Ternary diagram to illustrate advisable boundaries for minimum hazardous and maximum safe operation conditions to avoid explosion in CCGT and CCGE model experiments with H_2/CH_4 /CO fuel mixtures in air.

Some interesting evidence derives from these results and presentations.

(i) The laboratory tests of WP2.1 have demonstrated some important differences between the binary systems of H_2/CH_4 and H_2/CO. Whereas the reactivity of the former appears to be a linear function of the concentration ratio, that for the hydrogen/carbon monoxide system demonstrated a disproportionate enhanced reactivity as result of hydrogen addition, which became apparent before the 50/50 mix was reached.

(ii) Scaling up to the cylindrical duct, results of WP2.2 bear out the same evidence. In Figure 1.a the lines of constant fuels ratio for H_2/CH_4 run more or less parallel as do the linear boundaries of the “safe” and “unsafe” planes concentration planes in Figure 2. By contrast, these boundaries are curved in Figure 2, while in Figure 1 the H_2/CO lines converge with those for 100% H_2, except for 100% CO. The extent of this coalescence is shown in Table 2. Clearly, hydrogen has a special activating influence on carbon monoxide, which from the equi-molar concentration makes their combined reactivity virtually indistinguishable from that of pure hydrogen. As Figure 1.c and Table 2 show, the presence of even 25% CH_4 seems to have little effect on this and a more fundamental study of this behaviour is fully justified.

2 THE INFLUENCE OF HEAT EXCHANGER MODEL OBSTRUCTIONS ON THE CHARACTER OF COMBUSTING FLOW.

2.1 In Section 1, the information from the Part 1 of this report “ETI WP2, Task 2, Experimental results (MH_15_138)” was used for a general determination of hazardous and relatively safe operating equivalence ratios for the model H_2/CH_4/CO fuel mixtures in their various concentrations. These have also been summarised in Figure 2. This result was obtained making use of the results of almost all WP2.2 tests 1 – 61. However, dealt with in this way, using maximum and average over-pressures recorded, the results do not fully consider the nature and therefore the role and potential hazards from flame development under the varying conditions or compare the dependence of its unobstructed progress with its character in the presence of obstructing heat exchanger models of varying length/depth.

To achieve this a more detailed analysis of the evidence of a limited number of tests that highlight this difference between free and obstructed flame development for fuel mixtures of constant composition and varying equivalence ratios in the oxygen enriched turbine exhaust flow.

For this purpose primary list of 16 tests were identified from the 61 performed at low flow inlet velocity and constant inlet temperature, for which the results could be compared with those of at least one other test at a different obstruction level but with the same equivalence ratio ($\varphi \pm 0.01$). The latter margin was judged to be within the accuracy with which equivalence ratios could have been determined. Collectively, this selection provided the 7 comparative sets, shown in Table 3, of which 2 incorporate all three of the obstruction levels investigated in the WP2.2 test programme. From the Experimental Report data the recorded maximum over pressures (Δp) and evaluated flame velocities (v_{flame}) are also listed.

As shown, the sets are not ordered around set mixture compositions, but on the basis of increasing over-pressure and flame speed of the un-obstructed test mixture. Where more than one number is shown as “XX/YY” the different maxima relate to the output from two different sensors along the length of the WP2.2 circular duct rig. In some instances the differences appear not to be from process variations, but due to malfunction of one of the two recording sensors.

Table 3: Test mixtures selected from the WP2.2 test programme best suited to investigate the influence on over-pressure and flame velocity on combustion in the CCGT and CCGE model arrangements of WP2.23

	No Obstruction			8 tube rows			15 tube rows		
	Run	Δp	vflame	**Run**	Δp	vflame	**Run**	Δp	Vflame
	[No]	[mbar]	[m/sec]	[No]	[mbar]	[m/sec]	[No]	[mbar]	[m/sec]
H_2/CH_4 60/40; φ=0.35	**13**	43	63/0	**19**	75	49			
H_2 100%; φ=0.42	**9**	73	0/93				**28**	451	167
H_2/CO 40/60; φ=0.50	**16**	91	0/90				**52**	824	286
H2 100%; φ=0.52	**10**	130	0/115	**24**	323	123	**27**	1733	416
H_2/CH_4 60/40; φ=0.66	**5**	168	169/170	**20**	591	353	**31**	3016	556
H_2 100%; φ=0.63	**26**	1050	(288?)				**29**	7159	1754
H_2 100%; φ=0.72	**11**	320	312/348	**25**	7620	1944			

The immediate and obvious evidence from the above is that, regardless of the fuel mix, the maximum over-pressures and flame velocities generated depend directly on the presence and extent of obstruction in the WP2.2 circular duct.

2.2. Problems in the way of a comprehensive analysis based on all data collected.

2.2.1. As presented in the Experimental Report, the results from the tests referred to in Table 3 were found not to be suitable for a detailed and accurate analysis of the combustion enhancing influence and effects from the model heat exchanger on the enriched turbine exhaust flows. The reasons are in part structural, in part related to the manner of presentation in the Experimental Report. It must be added that, while obvious now, these barriers to optimal result analysis were in many ways ‘unforseeable’, mainly because of inadequate up-front experience with the extensive and complex recording and analysing system.

2.2.2. As for the structural problems: because of the very large number of sensors required and the significant cost of having these purchased (if

available), all except the pressure sensors were ‘custom-made’. However, despite best design and manufacturing efforts, the ionisation probes proved not to be as reliable as intended, especially in the earlier tests. Understandably also affected by low ionisation levels for slow and marginal combustion and combined with the difficulties of this large and complex rig, information from probes was for some of the more challenging tests less than 50%, leaving significant information gaps for the overall understanding required. As for the optical probes: their initial design proved not fully successful in excluding stray and advancing source light. Additionally, interaction between sensors outputs, and signal overlap and signal noise could make identification of individual signals an arduous and lengthy task.

The provision of arrays of different types of sensors was intended to provide detailed comprehensive rather than just supplementary information on a number of distinctive details of flame development. To do this efficiently the positions of at least two different types of sensors should have coincided at a satisfactory number of locations with respect to the long axis of circular duct. Given the available resources and the need to collect information along the full length of the 12 m long duct, such opportunities were limited: with mostly separated positions, the combined individual information on a normally changing flame process could not readily be interpreted coherently. Having said this, at four distances from the point of ignition the axial location of an ionisation probe aligned with that of a pressure transducer and at two positions did they coincide with the plane of view of an optical probe. The latter is unfortunate as first responses in the optical probe records to the ignition are mostly at variance with that of the other sensors, while the response signals could be viewed as not well defined. The latter is in part a result of the light reflections in the recesses that house the sensors; in part it is also clearly due to signal input overload. With hindsight it must be admitted that - because of design or installation imperfections - predominantly complementary rather than comprehensive information could readily be obtained, which is a lesson for the WP2.3 programme.

2.2.3. Additionally, as already pointed out in the Part 1, Experimental Report, the time-bases of the pressure and optical sensors did not accurately agree with that of the ionisation probes. This is due to the individual characteristics of different cards in the recording system.

2.2.4. Thus the suitability of the Experimental Report data for combustion analysis, was adequate for the more *general* evaluations of Section 1, where identification of maximum and acceptable over pressures anywhere in the WP2.2 facility was required to determine too hazardous and relatively safe operating conditions for the $H_2/CH_4/CO$ fuel mixtures. However, for *detailed* analysis of combustion behaviour the results from the Experimental Report needed to be reviewed and adjusted. Specifically, to achieve the necessary accuracy improvements were required, including:

1. For Section 1, mean flame velocities were quoted and graphically shown at the end of a distance interval over which these had been calculated rather than the mid-distance point;
2. locations of maximum overpressures were time markers, rather than the onset of pressure rise, which in particular for sonic pressure waves indicates the arrival of the ‘combustion wave’ and is for combustion progress assessment the important moment;
3. software analysis of the data could show ionisation probe responses preceding the arrival of the pressure wave, which is scientifically unsound;
4. the times of optical sensor responses sometimes precede those of other sensors at an upstream position;
5. optical probe and pressure transducer responses are frequently distorted because of interference from the response from earlier sensors in the same group, which commonly lifts the baseline;
6. downstream of the heat exchanger model location, the distances of sensors to the beginning or ignition point of the circular duct needed to be increased by 100 mm allowance for the width of the flange that supported the heat exchanger tube holder.

2.2.5. For the more detailed analysis and interpretation, that would highlight the nature of the combustion process and in particular conditions or locations for its enhancement, the causes for such discrepancies first had to be identified and the relevant data from the Experimental Report improved.

Following early discussion between members of the Consortium this was attempted by considering the data output files from the tests, where possible and necessary, by trying to adjust the data and to see whether from this a coherent image of flame development for the particular test could be extracted. Unfortunately, despite very extensive trying, this was not achieved with the available data set because of clarity and accuracy of signals and/or the problems outlined in the points of para 2.2.4. It was concluded that only a complete new analysis and inter-comparison of all the sensor outputs from the tests of interest might be able to provide the information and insight required. The procedures for this are outlined below in Section 3 and Appendix A.

3 DETAILED ANALYSIS OF TASK 2 EXPERIMENTAL DATA.

3.1. The basis required for a more detailed analysis and understanding of flame development and its hazards in a free or obstructed facility such as the circular duct model facility of WP2.2 has to be a clear and sufficiently accurate display of the distance versus time progression of the flame front. Once this is obtained, additional information on the flame front, flame structure and overpressures generated can be obtained from contributing responses of the different types of sensors employed. In turn this can then be interpreted in the light of the compositions and conditions of the mixture investigated and the influence of the confinement and obstructions of the test facility.

This adaptation of the Experimental Report (ER) data-set for more ‘advanced’ analysis has been carried out for five selected tests from those listed in Table 3.

The successive data evaluation steps required for such an optimal analysis and interpretation of the ER results in terms of revealed combustion behaviour are complex and are described in Appendix A for Test 27. This test was one of the 100% H2 tests, which with a heat exchanger model obstruction of fifteen rows of pipes caused flame velocities and over- pressures suggestive of part-detonative behaviour.

4 RESULTS: CONSTRUCTION OF DISTANCE VERSUS TIME DIAGRAMS.

4.1 With the creation of these best achievable time data, there remain two further requirements to enable display of distance vs time functions.

The first is the listing of sensor positions. This requires,

(a) for appreciation of overall upstream combustion development and function creation: distances of probe positions to the point of ignition,

(b) for appreciation of overall downstream combustion development and function creation, distances to the first sensor downstream of the heat exchanger model

(c) for estimates of local flame velocities and flame development within the areas of (a) and (b), inter probe distances.

The second are time differences for each of the distances listed under (a) – (c).

In the first instance, this report has focussed on creating the database from which all above options can readily be developed and a relatively accurate graphical oversight can be given. To this end distances to point of ignition from Experimental Report data and time intervals from Table A1.1 (Appendix A), column 4 less column 1, are respectively listed in columns 5 and 6. In the former, the inter-probe distances are also given. These last two tasks are also summarised by Figure A1.1 (see Appendix A), boxes 12 and 13.

4.2 Completion of Table A1.1 then finally allows construction of the distance vs time diagram. For all 5 tests discussed in this first report such diagrams and the results of such parallel calculations as detailed in Section 3 are shown as follows:

- Test 10: 100% H_2 at φ = 0.52, & no HE model; Figure 4 and Appendix B

- Test 24: 100% H2 at φ = 0.52, & 7 row HE model: Figure 5 and Appendix C

- Test 27: 100% H_2 at φ = 0.52, & 15 row HE model: Figure 6 and Appendix A

- Test 29: 100% H_2 at φ = 0.63, & 15 row HE model: Figure 7 and Appendix D

- Test 25: 100% H_2 at φ = 0.72, & 7 row HE model: Figure 8 and Appendix E

5 EVALUATION OF RESULTS.

5.1 **The results show that the very methodology of the analysis of this report has paid off. The number of 46 NS (no signal) and NA sensor responses for the five 5 Tests in the Experimental report (28%) - see section 3, point 2 - has been reduced to ONE (0.6%).**

5.2 The slopes of straight lines drawn by eye through the results indicate approximate overall velocities of the pressure and/or combustion waves. These demonstrate the validity of scaling approach used, the test mixtures selected for Task 2 building on the findings of the laboratory experiments carried out in Task 1. The success of this approach gives confidence for the next stage in the Task 3 HRSG rig.

5.3 For these 100% H_2 tests the undisturbed flame (Test 10) and therefore the flame upstream of the HE model (other tests) develops very much according to expectation. With an increase in the equivalence ratio from about 0.5 to 0.7 the overall flame velocity rises from approximately 80 to 120 m/sec.

5.4 The diagrams of the HE model constrained tests, e.g. Tests 24 and 27, Figures 5 and 6 show that a linear extrapolation of the correlation line back to the ignition point does not go through the diagram origin. This is as it should be because the flame needs some distance to accelerate from 0 – approximately 80 m/sec.

5.5 The very early pressure sensor responses, e.g. Tests 10 and 24, Figures 4 and 5, are records of the passage of the pressure wave caused by the initial explosion and the expanding initial flame.

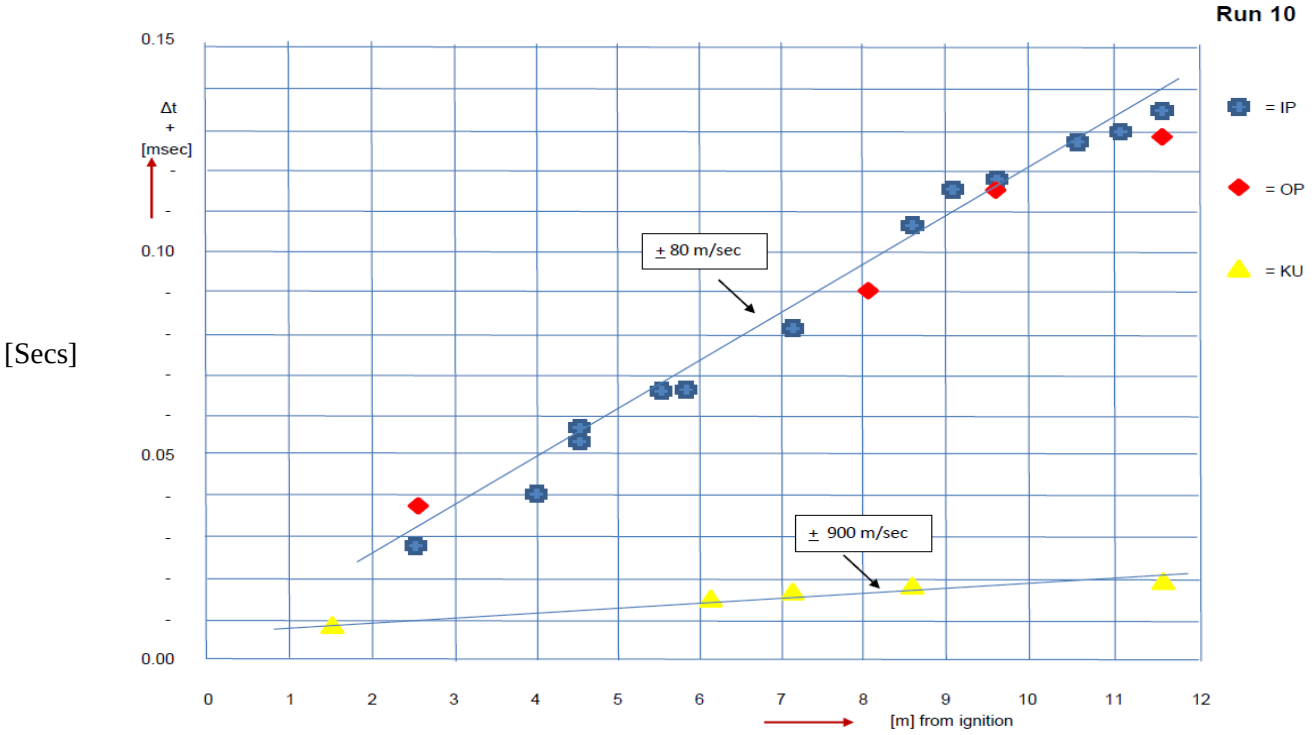

Figure 4: Distance vs Time for 100% H_2 at φ = 0.52 and no heat exchanger

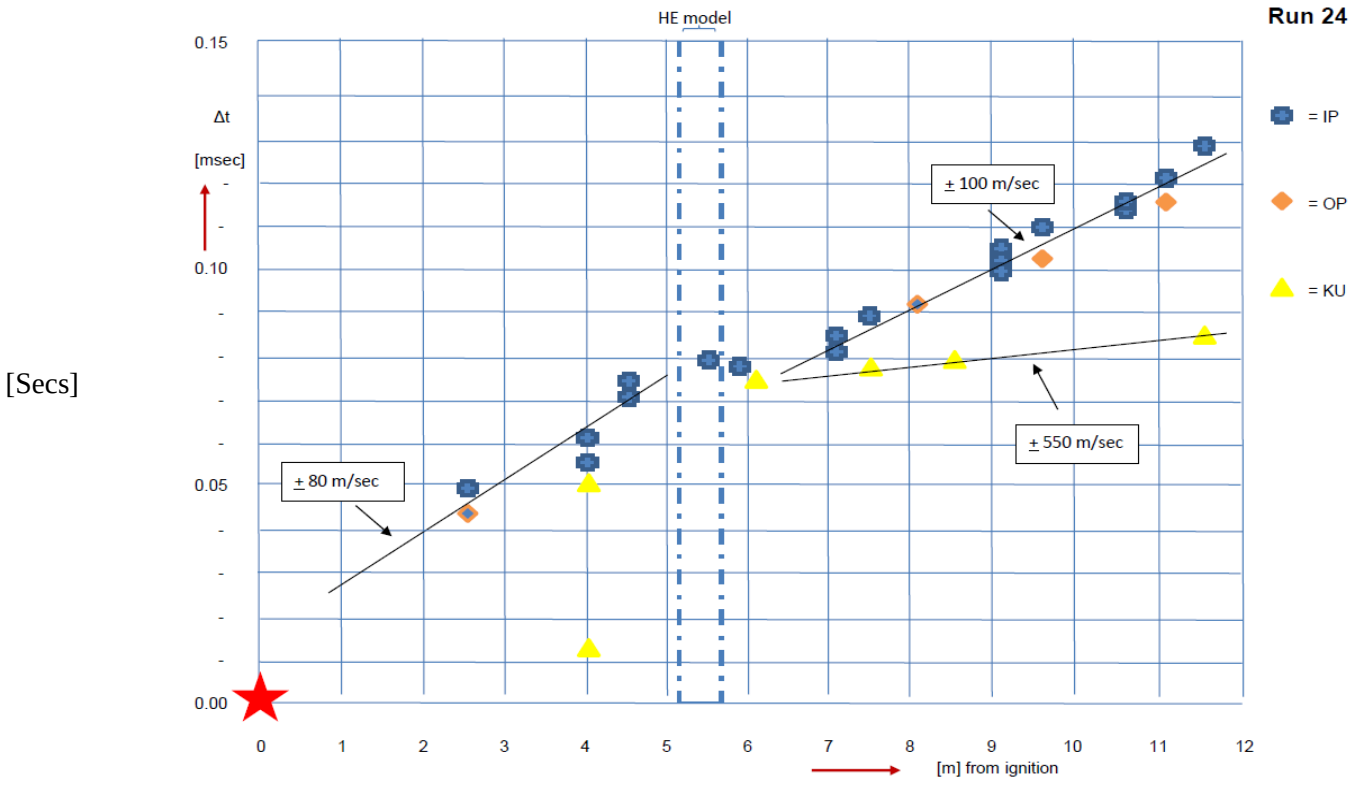

Figure 5: Distance vs Time for 100% H_2 at φ = 0.52 and 7 row heat exchanger

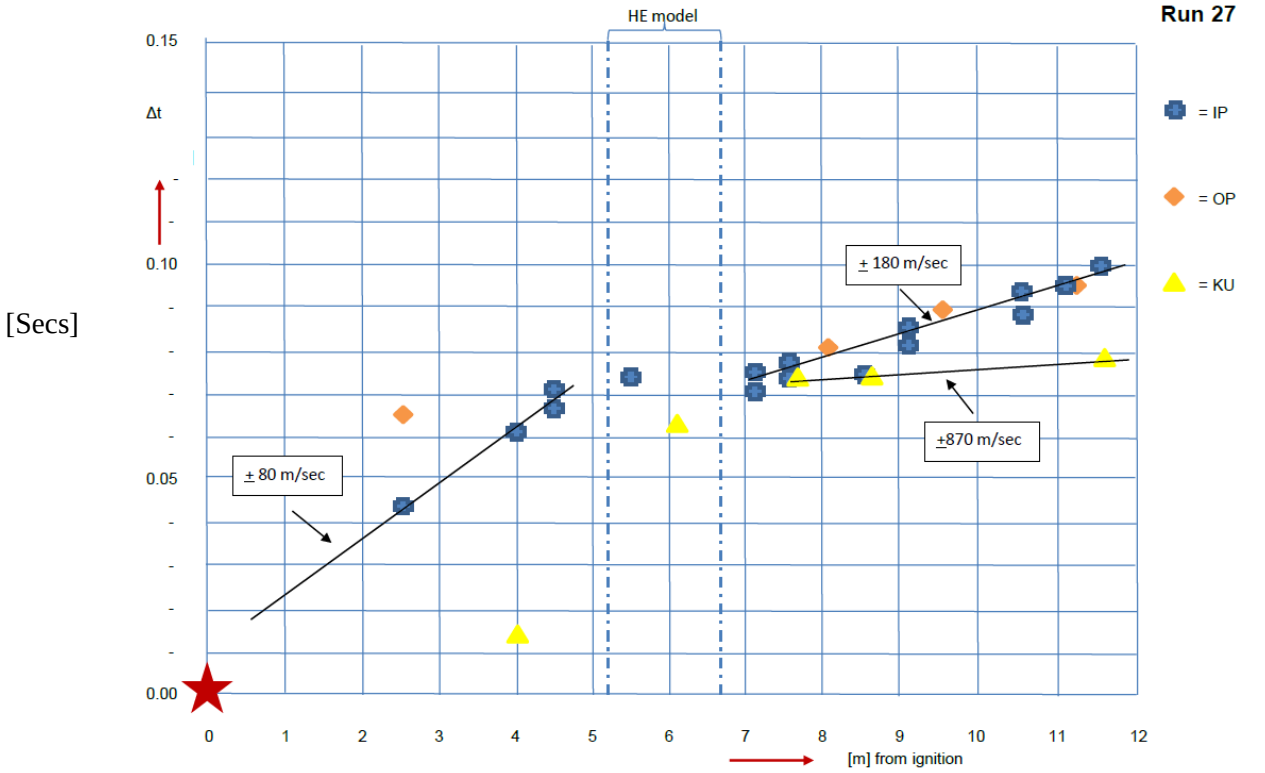

Figure 6: Distance vs Time for 100% H_2 at φ = 0.52 and 15 row heat exchanger

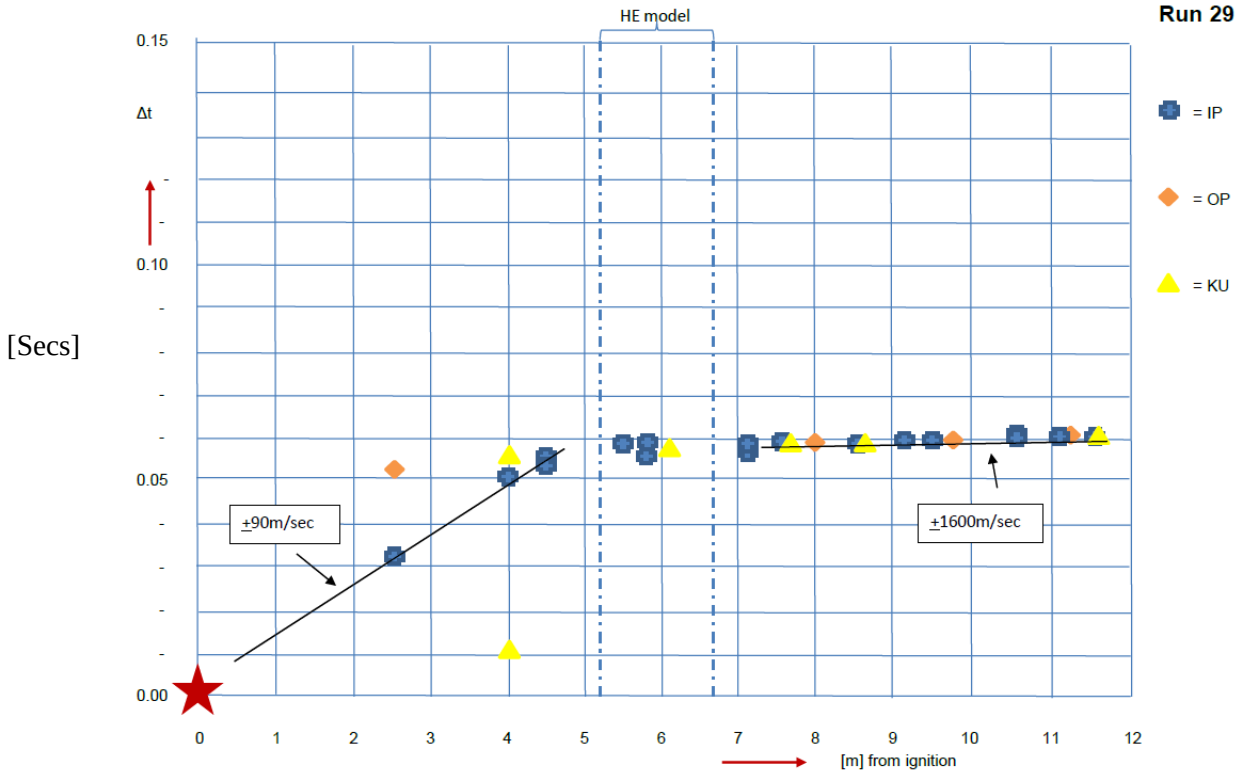

Figure 7: Distance vs Time for 100% H_2 at φ = 0.63 and with 15 row heat exchanger.

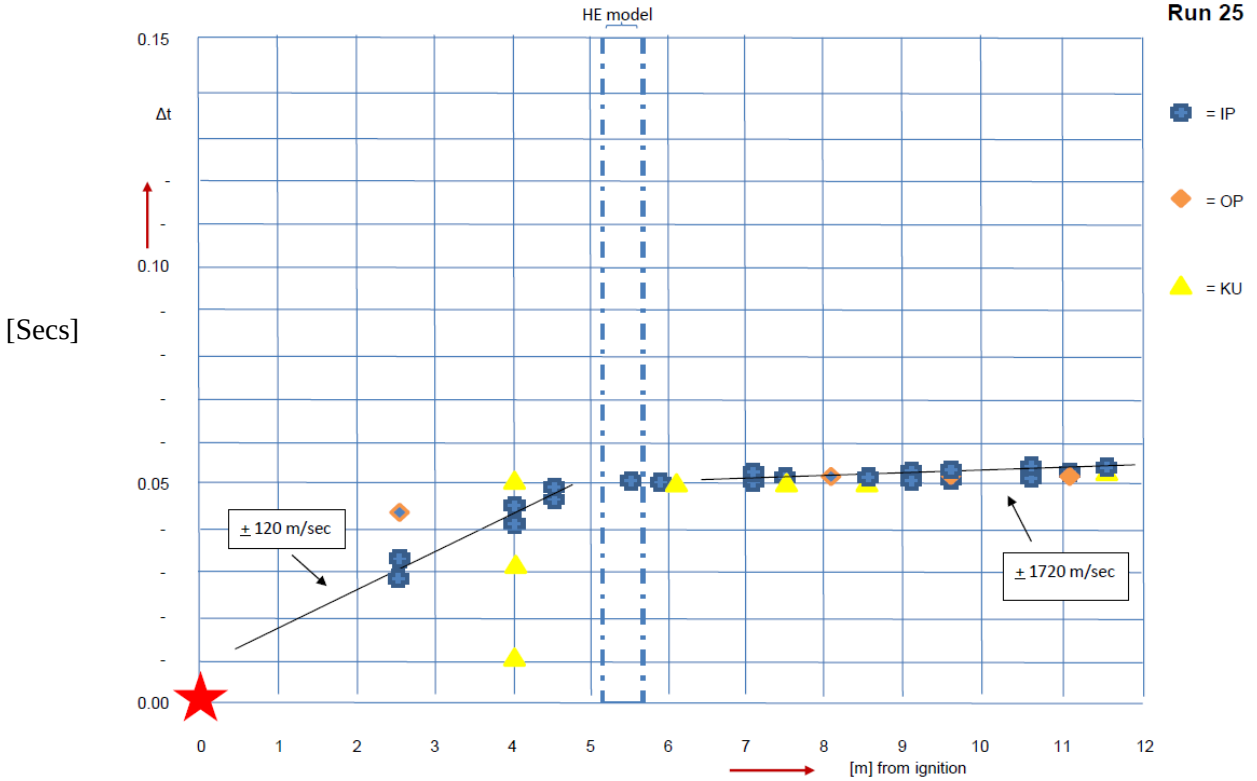

Figure 8: Distance vs Time for 100% H_2 at φ = 0.72 and with 7 row heat exchanger

5.6 The flame velocity "jumps" to extremely high levels in the HE model; it could in all obstructed instances be represented by a horizontal line. In part this is due to gas velocity increase by the blockage ratio of 40%+, much more due to the effect that the blockage and associated turbulence have on the combustion process which translates to a very powerful explosion.

5.7 On exiting from the HE model, the diagrams show that the flame fronts first slow down, see e.g. IP responses in Tests 24 and 29. This is fully consistent with previous experience [Lindstedt and Michels, Comb. and Flame 76: 169-181 (1989)] and is in part due to the reverse of effects indicated in para 5.6.

5.8 What happens thereafter depends on the energetics of the explosive mixture and the length = effect of the HE model. When If high enough, the shock from the intensely powerful gas release and explosivity exiting the HE model will set off a detonation process with shock wave, ionisation and combustion following each other very closely as shown for Test 29 (φ ≈ 0.7) by the close proximity of the outputs from the three types of sensors and the overall combustion velocity of around 1700 m/sec. It is also consistent with the maximum over-pressure recorded of 7 - 8 bar.

5.9 When the length of the HE model is reduced, i.e. a 7 row HE model, but all other conditions remain the same, its impact on the same 100% H_2 mixture is clearly less severe, see Test 24, Figure 6. After the temporary velocity fall at

exit (para 5.7) the flame will accelerate again but the less intense and slower pressure wave (~ 550 m/sec) fails to support the flame sufficiently and decouples, while the flame continues at its own enhanced but overall subsonic flame velocity of around 100 m/sec.

5.10 In Section 1 of this report it was concluded that for a particular fuel mixture a safe operating gap between a “lowest hazardous” and “highest safe” concentration in air would be $\Delta\varphi = 0.2$, see Table 2. For 100% H_2 these levels were respectively $\varphi_{haz} = 0.55$ and $\varphi_{safe} = 0.35$. Detailed analysis of the results actually confirms that **what really matters is to ensure that for a given size, type and length of heat exchanger the fuel mixture is not so energetic that it will generate an overpressure/shock at the exit that is powerful enough to auto-ignite the mixture sufficiently rapidly for a detonation type reaction to be maintained**. Test 27 (Figure 6) shows that for 100% H_2 and the 15 row heat exchanger the hazardous limit is indeed at $\varphi = 0.52 + 0.01$, where the near-exit over-pressure of 0.8 bar (KU3) was not able to set up a detonation, which resulted in a maximum recorded downstream over pressure of 1.7 bar (KU4 and Table 1).

We have as yet no similar telling results for the 7 row heat exchanger but **it will be very important for the WP2.3 test programme that the over-pressure at the exit of the heat exchanger can be recorded and monitored. The recommended safety margin of $\Delta\varphi = 0.2$ remains reasonable.**

6 FURTHER SUGGESTED WORK

6.1 The above are early appreciations of the enhanced results and further development and interpretation will follow. The first task will be to transfer the data from the appendices to excel spreadsheets so that curve fitting can take place and the overall velocity correlations be expressed as functions for future use. The sheets will be formatted to allow also for velocity calculation over shorter distances/time intervals and to incorporate the over-pressure values recorded. The velocities calculated will be averages and must therefore be assigned to the half-way point of the length interval for which they have been calculated.

Results from other tests in Table 3 that should/will be analysed in the same way include:

- the set of Tests 5, 20 and 31 for the H2/CH4 60/40 mixture is essential to look more closely at flame behaviour between the high risk and safe limits at the H2-CH4 boundary of the three dimensional model of Figure 2.
- and Tests 16 and 53 for the same purpose for H2/CO
- Analysis of the few lower temperature tests will also have to be conducted
- Results for the high gas velocity tests will first have to be considered as essential for completion of WP2.2 or as a preliminary for WP2.3

6.2 Finally on an ongoing basis, methods will have to be considered to see if this successful but time-consuming analysis method,

- Can be simplified and/or speeded up by using more cp based aid
- And/or remains necessary with the improvements that are being made in the detection and signal processing methods currently effected at the HSL.

6.3 In addition, the results obtained and the analysis achieved illustrate how the HRSG rig might be used post WP2.3 to understand the phenomena within the congested area, and the impact of different arrangements and systems (such as duct burners) on these phenomena as means of preventing or mitigating conditions that might lead to damaging overpressures.

7 APPENDIX A: DETAILED ANALYSIS FOR TEST 27

A1.1 This appendix describes the detailed analysis carried out, and understanding of flame development and its hazards in the free or obstructed circular duct model facility of WP2.2 for Test 27. The very thorough approach developed can be applied to other systems and data to produce a sufficiently accurate display of the distance versus time progression of the flame front. Additional information on the flame front, flame structure and overpressures generated can be obtained from contributing responses of the different sensor types, which can then further interpreted in the light of the compositions and conditions of the mixture investigated and the influence of the confinement and obstructions of the test facility.

The successive data evaluation steps required for such an optimal analysis and interpretation of the ER results in terms of revealed combustion behaviour are described in Appendix 1 for Test 27, which was one of the 100% H2 tests, which with a heat exchanger model obstruction of fifteen rows of pipes caused flame velocities and over- pressures suggestive of part-detonative behaviour.

The detailed approach developed is described in Figure A1.1; in what follows these are there also demonstrated for Test 27.

A1.2. As also shown in Table A1.1, the nature of the combustion process at various stages of the WP2.2 facility is directly related to the flame velocity. For this reason its evaluation requires accurate specification of distances and time at successive measuring positions with respect to the axis of the rig.

The *distances* used in this analysis are those given with the test results of the Experimental Report, except for two changes.

- The first is that - as pointed out in the last issue of the list of paragraph 2.2.4 - the in- and post-heat exchanger locations of the Experimental Report require adjustment for the 100 mm width of the flange supporting the heat exchanger model (and a ionisation probes rake). These changes have been incorporated.
- The second is that for flame development analysis, in first instance only the distances from the point of ignition matter. The location of the igniter was 250 mm from the leading end of the first straight 3 m section of the circular duct. All distances quoted from hereon have therefore been adjusted to this point.

Figure A1.1: How to construct a time/distance graph from results for WP2.2 test runs

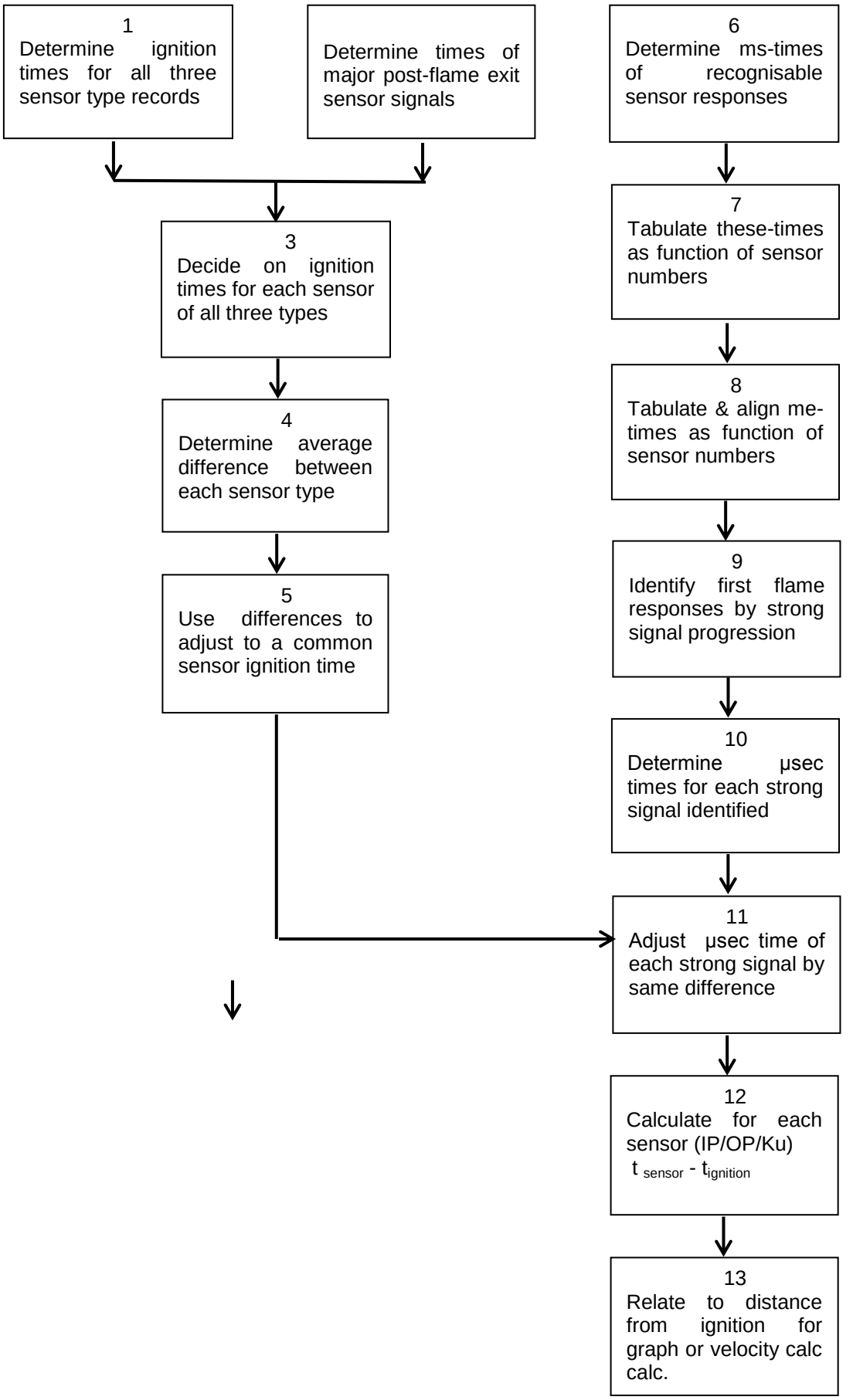

A1.3. The *time data* provided with the tests are taken from all related to the ER test records. Their last digit given was variably in the (0.1 – 0.01) millisecond range. As the minimum distance between two sensors downstream of the HE model is 0.5 m, this means that the highest flame velocities around 1700 m.s-1 could for such sections only be calculated with an accuracy of 30 (ms-1)? – 3%. It was therefore important to express all times to at least the lower value and also to review the accuracy of times provided by the recording system's time-base.

Maximum magnification of the Diadem TDMS records shows that for the ionisation probes the time between two successive peaks of the base signal is 20 microseconds, i.e. the positive and negative peaks of basic noise are separated by 10 microseconds. The moment of an event is not at the peak of a signal excursion above or below the width of the noise signal. The time of its arrival is when the sensor starts to respond to the change in external conditions. When this external input changes slowly, the sensor and recording system will follow it to its maximum value; when it is fast the rate of response is limited by the characteristics of sensor and/or recording system. When the signal is seen to rise positively above, respectively negatively drop below the preceding common maximum/minimum level of the noise signal band, the event will have arrived within the last half of the preceding noise excursion.

For ionisation probes this means that the initial sensor response indicates that the event arrived within the preceding 10 microseconds. Thus, by taking the arrival within that half cycle as occurring at the centre of the noise band width, the event arrival time for the ionisation probes can be determined with an accuracy of $\pm$ 5 microseconds. For the optical probes and pressure transducers the duration of the noise cycles were found to be approximately 35 microseconds; the accuracy of the output data for these sensors is therefore about $\pm$ 10 microseconds.

With this information, our analysis of the TDMS files can be illustrated with the example of Test 27.

A1.4. The first task listed at the top of Figure A1.1 was the determination of a common ignition time for all three sensors types employed. Like all such records there is an abundance of signals on each track, in about one quarter of cases half or completely obscured by the continuous output noise, when this is unfortunately relatively high compared to the strength of a sensor output. However, displaying a few sensor records simultaneously on the TDMS screen, a common single and sharp spike is usually readily found ahead of the first major peak and identified as the time of ignition. For test 27 such times in seconds, given to the microsecond digit, are shown in the first column of Table A1.1. As can be seen: the numbers for the ionisation probes are stable around 1.283 722, although gradually dropping by almost 20 microseconds.

Table A1.1: ETI WP2.2.Times [sec] Updates Run 27

Run	Ignition	Ignition l	Main Signal	Adjusted	Distance	Time	Final signal
	[sec]	adjust.		main signal	from previous/	from	
		[µsec]			ignition [mm]	ignition [sec]	
IGN	1.238 722	-2	1.238 722	1.238 720			
IP1	1.238 722		1.282 302	1.282 300	2500/2500	0.043 580	2.774 864
IP2	1.238 722		1.301 612	1.301 610	1500/4000	0.062 411	2.744 864
			1.314 383	1.314 381			2.744 864
IP3	1.238 722		1.306 502	1.306 500		0.067 780	2.744 864
IP4	1.238 722		1.305 972	1.305 970	500/4500	0.067 250	2.744 864
IP5	1.238 722		1.310 802	1.310 800		0.072 080	2.744 864
……							
IP6	1.238 722		1.314 637	1.314 635	1000/5500	0.075 915	2.744 864
IP7	1.238 722		1.314 002	1.314 000		0.075 280	2.744 864
IP8	1.283 722		1.314 002	1.314 000	300/5800	0.075 280	2.744 863
IP9	1.283 722		1.314 002	1.314 000		0.075 280	2.744 863
……							
IP11	1.283 722		1.314 742	1.314 740		0.076 020	2.744 863
IP12	1.283 722		1.312 562	1.312 560	1300/7100	0.073 840	2.744 863
IP13	1.283 722		1.315 068	1.315 066		0.076 346	2.744 863
IP10	1.283 719	+1	1.313 349	1.313 350	500/7600	0.074 630	2.744 863
			1.317 233	1.317 234		0.078 514	
IP14	1.283 720			1.314 529	1000/8600	0.075 809	2.744 863

IP15	1.283 720		1.322 620	1.322 636	500/910	0.083 916	2.744 863
			1.326 899	1.327 000		0.088 280	
IP16	1.238 704	+16	1.322 594	1.322 610		2.744 842	2.744 842
			1.325 794	1.325 810		0.087 090	
IP17	1.238 704		1.322 620	1.322 636		0.083 916	2.744 842
			1.326 128	1.326 144		0.087 408	
IP18	1.238 704		????????		500/9600		2.744 842
			1.329 107	1.329 123	1000/10600	0.090 403	
IP19	1.238 704		1.327 906	1.327 922		0.089 202	2.744 842
			1.333 564	1.333 580		0.094 860	
!P20	1.238 704		1.328 012	1.328 028		0.089 308	2.744 842
			1.332 695	1.332 711		0.093 991	
IP21	1.238 704		1.327 996	1.328 012			2.744 842
			1.333 686	1.333 702		0.094 982	
IP22	1.238 704		1.335 568	1.335 584	500/11100	0.096 864	2.744 842
IP23	1.238 704		1.338 546	1.338 562	500/11600	0.099 842	2.744 842
OP0``	1.238 349	+371	1.304 900	1.305 271	2500/2500	0.066 551	2.744 510
OP1	1.238 349		1.318 100	1.318 471	5600/8100	0.079 751	2.744 510
OP2	1.238 342		1.326 468	1.326 839	1500/9600	0.088 119	2.744 510
OP3	1.238 340	+380	1.333 446	1.333 835	1500/11100	0.095 115	2.744 510
KU0	1.238 350	+370	1.253 350	1.253 720	4000/4000	0.015 000	2.744 510
KU3	1.238 344	+376	1.301 900	1.302 276	2100/6100	0.063 556	2.744 503
KU5	1.238 344		1.312 000	1.312 376	1500/7600	0.073 656	2.744 502
KU6	1.238 344		1.313 935	1.314 311	1000/8600	0.075 591	2.744 503
KU7	1.238 344		1.317 740	1.318 116	3000/11600	0.079396	2.744 503

A1.5 Another reliable comparison of the time records of the three types of sensors could be obtained from the massive signal that appears on all time-records after the combustion front has passed IP 23 and must have exited the duct. The delay varies from test to test in a 50 – 1000 msec range. Leaving aside the cause of this impact on the recording system, it was found that – as readily appreciated - this occurred also at exactly the same time for each of the three sensor types. Given its strength and clarity, this signal is an alternative reference for harmonising the ignition times and hence the time records of the different sensor sets. This alternative is summarised in the second box of A1.1. The choice is represented by box 3 in Figure A1.1, which in our case was made to be the direct ignition time reading from the Diadem TDMS file at maximum magnification.

A1.6 Whichever option was chosen, the next step in the analysis, represented by box 4 in Figure A1.1, was to check for any differences in event recording times between the pressure and/or optical sensors and the ionisation probes. As mentioned in para 2.4.4 of the main text, it had already been established by the HSL test team that the real time ignition moments for the various sensors employed are not aligned, which was ascribed to the characteristics of individual cards in the separate recording systems employed. The signal available for comparison is the pick-up from the condenser discharge that causes ignition. From this and analysis of time records of all Test 27 sensors, *average* ignition times are approximately

- Ionisation probes: 1.283 715 sec $\pm$ 10 µsec
- Optical probes: 1.283 345 sec $\pm$ 5 µsec = IP time less 370 µsec
- Pressure sensors: 1.283 346 sec $\pm$ 4 µsec = IP time less 369 µsec.

Note that the variations are genuine and systematic and are not the uncertainties of para A1.3 above.

A1.7. For the purpose of a detailed and comprehensive analysis and interpretation of the experimental results, these time records of data and therefore the ignition times recorded by individual sensors needed to be brought in agreement (Figure A1.1, Box 5) For our evaluations time difference rather than absolute time is important, as is also to retain a point of reference with the information from the Experimental Report. In the analysis of all test results except those of Test 5, the output data from all three sensor types were therefore adjusted to agree with those of the (ionisation probe) ignition record of Test 27 shown in the Experimental Report, which was 1.283 470 seconds. Thus the ignition and sensors response times given above would *on average* have to be adjusted as follows:

- Ionisation probes: 1.283 715 sec + 5 µsec = 1.283 720 sec
- Optical probes: 1.283 345 sec + (370 + 5) µsec = 1.283 470 sec
- Pressure sensors: 1.283 346 sec + (369 + 5) µsec = 1.283 470 sec.

In practice it was preferable to consider individual corrections for each sensor. Thus for all Test 27 ignition time records obtained from the Experimental Report the following *actual* additions had to be made in the following ranges:

- Ionisation probes: + -2 to + 16 µsec
- Optical probes: + 371 to 380 µsec
- Pressure sensors: + 385 µsec

The appropriate corrections are listed in the second column of Table A1.1.

A1.8. With a common ignition time agreed, progress needed to turn to an agreement on times of sensor responses to the passage of the flame so that these can be used for a more fundamental analysis: this has been the main problem in using the test results from the Experimental Report. A summary of reasons for this includes:

- Difficulties to derive from a single set of the time data given a consistent in picture of flame development, especially upstream of any HE insertions;
- the number of NS (no signal) and NA responses, varying from 3/32 sensors (test 25) to 23/32 (test 10; no ionisation probe responses);
- the limited accuracy for higher velocities;
- the occasional inconsistency between signal sequence and expected flame development, although this may have been caused by a strongly deformed flame front;
- the disagreement between response times from the few aligned different types of probes; this includes optical probe responses preceding signal from pressure transducers, which is difficult to comprehend;
- the use of times of maximum sensor outputs which takes no account of the difference in time-width

A1.9 Unable to accommodate all these issues in re-arranging the Experimental Report data, it was ultimately decided to start to the effort from fresh and the procedure followed is summarised in the right hand column of Figure A1.1, starting with box 6 and 7

First the output signals of all ionisation probes in individual TDMS Test matrices were scanned at Diadem intermediate magnification from ignition time to the response of the last sensor IP23. First noticeable deflection of each strong and evident signal recorded with to an accuracy of one millisecond. In Table A1.2.a such data are listed for Test 27. By bold print these strong signals were provisionally identified as likely primary sensor responses. For about 20% of sensors even the most important signal could be hidden in the noise. In some instances it was not possible to find an identifiable signal. The data were placed in rows associated with rising IP numbers (box 8).

Given that the three ionisation probes on rakes were likely to have closely similar response times, such sets of responses would then be assumed to also represent flame passage and shown in bold print, although on occasions such sets could demonstrate agreement around more than one time, sometimes close to another set.

Table A1.2.a WP2.2 Run 27; matching IP sensor response times

IP1	**1.295**	**1.370**						
IP 2	1.302							
IP 3	1.306	1.311						
IP4	1.305	1.311	1.332					
IP5	1.295	1.311	1.312	1.322	1.333			
IP6	1.292	1.302	1.307	1.314	1.320	1.334		
IP7	1.292	1.313	1.317	1.337	1.343	1.356	1.363	1.370
IP8	1.311	1.314						
IP9	1.311	1.315	1.342					
IP11	1.315	1.319	1.323					
IP12	1.313	1.319	1.324					
IP13	1.315	1.319	1.323					
IP10	1.313	1.317	1.321					
IP14	1.320	1.339	1.347	1.372				
IP15	1.323	1.327	1.339	1.347	1.371			
IP16	1.315	1.323	1.326	1.334	1.349	1.358	1.372	
IP17	1.315	1.323	1.329	1.338	1.348	1.372		
IP18	1.315	1.329	1.337	1.347				
IP19	1.329	1.333	1.348	1.360	1.373			
IP20	1.310	1.320	1.326	1.333	1.342	1.345	1.361	1.374
IP21	1.310	1.320	1.328	1.333	1.345	1.360	1.374	
IP22	1.335	1.347	1.375					
IP23	1.338	1.348	1.360	1.374				

Table A1.2.b: Run 27; matching IP sensor response times

IP1	**1.295**																	1.370
IP 2		**1.302**																1.381
IP3			**1.306**		1.311													
IP4			**1.305**		1.311					1.332								
IP5	1.295		**1.311**		1.312			1.322			1.333							
IP6	1.292		1.302	**1.307**	1.314			1.320					1.334					
IP7	1.292				**1.313**	1.317							1.337	1.343		1.356	1.363	1.370
IP8					**1.311**	1.314												
IP9					**1.311**	1.315								1.342				
IP11						**1.315**	1.319	1.323										
IP12						**1.313**	1.319	1.324										
IP13						**1.315**	1.319	1.323										
IP10						1.313	**1.317**	1.321										
IP14								**1.320**					1.339		1.347			1.372
IP15								1.323	**1.327**				1.339		1.347			1.371
IP16						1.315		1.323	**1.326**		1.334				1.349	1.358		1.372
IP17						1.315		1.323	**1.329**				1.338		1.348			1.372
IP18						1.315				**1.329**			1.337		1.347			

(Commercial)

IP19										1.329	**1.333**				1.348	1.360		1.373
IP20					1.310			1.320		1.326	**1.333**			1.342	1.345	1.361		1.374
IP21					1.310			1.320		1.328	**1.333**				1.345	1.360		1.374
IP22												**1.335**			1.347			1.375
IP23													**1.338**		1.348	1.360		1.374

All millisecond results would then be aligned in columns of closely similar sensor response times, bearing in mind that in any event the times would have to rise with the increase of the IP number. By trial and error this would then produce a table of matching response times (box 9), such as also illustrated for Test 27 in Table A1.2.b. From this the bold figures would then be provisionally assumed to be the correct flame arrival time at the probe of the respective table row.

A1.10 For each of the ionisation probes the probe signal record was then scanned again at Diadem maximum magnification to determine from the bold sensor time response and as closely the start of the combustion wave passage. Double expansion was used and time coordinates recorded to the microsecond digit. This part of the procedure is summarised in Figure A1.1, box 10; For Test 27 the results are given in Table A1.2, column 3. As shown, new high resolution results from optical and pressure sensors analysis have been added to the table. Deciding on the correct instant of the arrival of the combustion wave was however not straightforward and was guided by the following basic understanding.

A1.10.1. Whatever the state of flame propagation, at a sensor position the first sign of its approach should always be that of an increase in the *pressure sensor* signal. At sub-sonic flame velocities this is indicated by a slow/extended precursor rise caused by the volume increase of the combustion zone. This rise will become steeper and more significant the further downstream the sensor is positioned, due to the accumulation of the pressure waves. Arrival/passage of the combustion wave proper is identified by the onset of a much steeper pressure rise, which starts from the top of the local pressure precursor level. When velocity exceeds the local sound velocity by more than about 5+%, the pressure rise is effectively instantaneous, regardless of whether this is linked to a following detonation wave. Thus at sub-sonic combustion it is the additional rise to higher pressure levels that indicate the arrival of combustion and with sonic combustion the more or less instantaneous rise from a single shock.

A1.10.2. The next indicator is a response from an *ionisation probe*. This can have two forms. The main and common one is the detection of ionisation due to temperature rise caused mainly by radiation from the following combustion. This will promote continuing combustion once sufficient ionisation becomes available around 1500 K. However, ionisation starts well below that temperature and it depends on the sensitivity of the probe at what level it will respond.

When a shock is formed ionisation will also occur as result of the very rapid pressure and temperature rise that causes ignition, such as in a detonation. This precedes and will be followed by the response to the much higher ionisation levels in the following supporting flame. Thus ionisation sensors responses should always follow pressure sensors signals and a response from an ionisation probe is not an indication of the passage of the front of a combustion wave. In a detonation at initially ambient pressure the distance between the shock front and the first ionisation band can readily be 100 – 200 mm, but at relatively low flame velocities with negligible pressure rise it may be the first detectable indicator.

A1.10.3. Ideally, *optical sensors* should signal the passage of the combustion zone proper across its central line of view and are therefore used where a response

is sought from anywhere across the diameter of gas mixture containment. Unfortunately, they are extremely difficult to collimate and even deeply recessed are sensitive to reflections from upstream flames, triggering a response at times that occasionally are even ahead of that from a pressure sensor at the same location. Their best indicator of the moment of actual flame arrival is the point on the signal track where a gradually rising response suddenly takes on a much steeper slope as the flame proper gets into direct view.

Overall optical sensor records have been very problematic to interpret because of

- the early responses to reflected light,
- which may come from different sides of the duct
- and the complication that successive responses may not cause all track responses to head in the same direction.
- Additionally, the flame proper is of course always following the pressure front but without visual records there seems to be no reliable way to decide what the time or distance difference is.

We have found it very difficult to relate optical sensor responses to the more reliable time information and combustion wave velocity evaluations from the ionisation and pressure sensors. The optical sensors were intended to advise on flame passage across the diameter of the duct, but in the present work this has been much more reliably indicated by the ionisation sensors rake. A review of the design of optical probes has since taken place and their efficiency is being evaluated with the last duct inlet velocity tests.

A1.11. As indicated by Figure A1.1, box 11, the sensor response times of Table A1.1, column 3 must of course be adjusted and brought into agreement in the same ways and for the same reasons as outlined in paras 3.4 – 3.7. for the sensor ignition times. As illustrated in the table for Test 27, the corrections of column 2 have therefore also been applied to all individual readings of column 3 to result in the amended main signal times of column 4. Note:

- the three results evaluated for rake probes have been bracketed by accolades
- the position of the model heat exchanger is indicated by two horizontal dotted lines.
- IP 10 was consistently positioned further downstream than the rake containing IP 11,12 and 13.

8 APPENDIX B: DETAILED ANALYSIS FOR TEST 10

Appendix B: WP2.2.Start Times [sec] Updates Run 10

Run	Ignition [sec]	Ignition l adjust. [µsec]	Main Signal [sec]	Adjusted main signal	Distance from previous Or ignition [mm]	Time from ignition [sec]	Final signal [sec]
IGN	1.251 970	+ 10	1..251 970	1.251 980			2.783 460
IP1	1.251 970				2500/2500	0.028 171	2.783 460
IP2	1.251 970				1500/4000	0.043 804	2.783 460
IP3	1.251 970		1.305 356	1.305 366		0.053 386	2.783 460
IP4	1.251 970		1.309 899	1.309 909	500/4500	0.057 929	2.783 460
IP5	1.251 970		1.304 824	1.304 834		0.023 230	2.783 460
IP6	1.251 970		1.318 600	1.318 610	1000/5500	0.066 630	2.783 460
IP7	1.251 970		1.298 408	1.298 418		0.046 438	*2.783 460*
IP8	1.251 960	+20			300/5800		
IP9	1.251 960		1.317 600	1.317 620		0.065 640	2.783 452
IP11	1.251 960		1.339 400	1.339 420		0.087 440	2.783 450
IP12	1.251 960		1.339 000	1.339 020	500/7600	0.087 040	2.783 450
IP13	1.251 960		1.336 100	1.336 120		0.081632	2.783 451
IP10	1.251 960		1.333 935	1.333 955	1300/7100	0.081 975	2.783 451
IP14	1.251 960		1.358 660	1.358 680	1000/8600	0.106 700	2.783 451
IP15	1.251 960		1.380 410	1.380 430		0.128 450	*2.783 451*
IP16	1.251 950	+30	1.380 403	1.380 433	500/9100	0.128 453	*2.783 432*
IP17	1.251 950		1.380 410	1.380 440?		*0.128 460*	2.783 432
IP18	1.251 950				500/9600		2.783 432
IP19	1.251 950		1.380 871	1.380 901		0.128 921	2.783 432
!P20	1.251 950		1.380 670	1.380 700	1000/10600	0.128 720	2.783 432
IP21	1.251 950		1.380 665	1.380 695		0.128 715	2.783 431
IP22	1.251 950		1.381 623	1.381 653	500/11100	0.129 673	2.783 432
!P23	1.251 950		1.387 000	1.387 030	500/11600	0.135 050	2.783 432

9 APPENDIX C: DETAILED ANALYSIS FOR TEST 24

Appendix C: WP2.2.Times [sec] Updates Run 24

Run	Ignition [sec]	Ignition adjust. [µsec]	Main Signal [sec]	Adjusted main signal	Distance from previous Or ignition [mm]	Time from ignition [sec]	Final signal [sec]
IGN	1.450 620	+0	1.450 620				
IP1	1.450 620		1.500 437	1.500 437	2500/2500	0.049 817	2.946 702
IP2	1.450 620		1.507 000	1.507 000	1500/4000	0.056 380	2.946 702
			1.512 748	1.542 748		0.062 128	
IP3	1.450 620		1.527 000	1.527 000		0.076 380	2.946 702
			(Reflected? :	1.539 250			
IP4	1.450 620		1.526 745	1.526 745	500/4500	0.076 125	2.946 702
IP5	1.450 620		1.524 379	1.524 379		0.073 759	2.946 698
……							
IP6	1.450 620		1.529 793	1.529 793	1000/5500	0.079 173	2.946 700
……							
IP7	1.450 620		1.528 503	1.528 503		0.077 883	2.946 700
IP8	1.450 620		1.529 069	1.529 069	300/5800	0.078 449	2.946 685
IP9	1.450 620		1.528 838	1.528 838		0.078 218	2.946 685
IP11	1.450 620		1.534 937	1.534 937		0.084 317	2.946 685
IP12	1.450 620		1.535 152	1.535 152	1300/7100	0.084 532	2.946 685
IP13	1.450 630		1.535 288	1.535 288		0.084 668	2.946 685
IP10	1.450 620		1.540 208	1.540 208	500/7600	0.089 588	2.946 685
IP14	1.450 630				1000/8600		2.946 685
IP15	1.450 630		1.553 750	1.553 750		0.103 130	2.946 685
IP16	1.450 620		1.551 470	1.551 470	500/9100	0.100 850	2.946 683
IP17	1.450 620		1.556 000	1.556 000		0.105 380	2.946 683
IP18	1.450 620		1.561 545	1.561 545	500/9600	0.110 925	2.946 683

10 APPENDIX D: DETAILED ANALYSIS FOR TEST 29

Appendix D: WP2.2.Times [sec] Updates Run 29

Run	Ignition [sec]	Ignition l adjust. [µsec]	Main Signal [sec]	Adjusted main signal [sec]	Distance from previous Or ignition [mm]	Time from ignition [sec]
IGN	1.283 448	+22		1.283 470		
IP1	1.283 457	+13	1.316 616	1.316 629	2500/2500	0.033 139
IP2	1.283 456	+14	1.333 587	1.333 601	1500/4000	0.050 131
IP3	1.283 456	+14	1.336 199	1.337 013		0.053 543
IP4	1.283 456	+14	1.335 923	1.335 937	500/4500	0.052 467
IP5	1.283 456		1.337 429	1.337 443		0.053 973
……						
IP6	1.283 452	+18	1.341 770	1.341 788	1000/5500	0.058 318
IP7	1.283 451	+19	1.341 818	1.341 837		0.058 367
IP8	1.283 451		1.342 108	1.342 127	300/5800	0.058 657
IP9	1.283 451		1.342 081	1.342 100		0.058 630
……						
IP11	1.283 452	+18	1.342 169	1.342 188		0.058 718
IP12	1.283 444	+26	1.342 148	1.342 174	1300/7100	0.058 704
IP13	1.283 453	+17	1.342 123	1.342 140		0.058 767
IP10	1.283 452	+18	1.342 447	1.342 465	500/7600	0.058 995
IP14	1.283 448	+22	1.342 340	1.342 362	1000/8600	0.058 892
IP15	1.283 452	+18	1.343 341	1.343 359		0.059 871
IP16	1.283 442	+28	1.343 346	1.343 374	500/9100	0.059 876
IP17	1.283 451	+17	1.343 346	1.343 363		0.059 876

11 APPENDIX E: DETAILED ANALYSIS FOR TEST 25

Appendix E: WP2.2.Start Times [sec] Updates Run 25

Run	Ignition [sec]	Ignition l adjust. [µsec]	Main Signal [sec]	Adjusted main signal [sec]	Distance from previous Or ignition [mm]	Final signal [sec]
IGN	1.251 970	+ 0.000 010	1.251 970	1.251 980		2.783 460
IP1	1.251 970			2500/2500		2.783 460
IP2	1.251 970			1500/4000		2.783 460
IP3	1.251 970		1.305 356	1.305 366		2.783 460
IP4	1.251 970		1.309 899	1.309 909	500/4500	2.783 460
IP5	1.251 970		1.275 200	1.275 210		2.783 460
IP6	1.251 970		1.318 600	1.318 610	1000/5500	2.783 460
IP7	1.251 970		1.298 408	1.298 418		2.783 460
IP8	1.251 960	+0.000 020			300/5800	2.783 452
IP9	1.251 960		1.317 600	1.317 620		2.783 452
IP10	1.251 960		1.333 935	1.333 955	1300/7100	2.783 451
IP11	1.251 960		1.339 400	1.339 420		
IP12	1.251 960		1.339 000	1.339 020	500/7600	2.783 450
IP13	1.251 960		1.336 100	1.336 120		
IP14	1.251 960	1.358 660	1.358 680	1000/8600		2.783 451

IP15	1.251 960		1.380 410	1.380 430		*2.783 451*
IP16	1.251 950	+0.000 030	1.380 403	1.380 433	500/9100	*2.783 432*
IP17	1.251 950		1.380 410	1.380 440		2.783 432
IP18	1.251 950				500/9600	2.783 432
IP19	1.251 950		1.380 871	1.380 901		2.783 432
!P20	1.251 950		1.380 670	1.380 700	1000/10600	2.783 432
IP21	1.251 950		1.380 665	1.380 695		2.783 431
IP22	1.251 950		1.381 623	1.381 653	500/11100	2.783 432
!P23	1.251 950		1.387 000	1.387 030	500/11600	2.783 432
OP0	1.251 605	+0.000 375	*1.288 743*	1.289 118	2500/2500	2.783 110
OP1	1.251 594	+0.000 386	*1.341 715*	1.342 101	5600/8100	2.783 100
OP2	1.251 593	+0.000 387	*1.365 931*	1.366 318	1500/9600	2.783 100
OP3	1.251 591	+0.000 389	*1.379 780*	1.380 169	2000/11100	2.783 100
KU0	1.251 590	+0.000 390	1.260 220	1.260 610	1500/1500	2.783 100
KU3	1.251 590	+0.000 389	1.267 686	1.268 075	4600/6100	2.783 100
KU5	1.251 592	+0.000 388	1.269 443	1.269 831	1000/7100	2.783 100
KU6	*1.251 593*	+0.000 387	1.270 625	1.271 012	1500/8600	2.783 110
KU7	*1.251 597*	+0.000 383	1.271 800	1.272 183	3000/11600	2.783 110

(Commercial)